Shiitake spent mushroom substrate as a sustainable feedstock for developing highly efficient nitrogen-doped biochars for treatment of dye-contaminated water

Alejandro Grimm [a,*], Glaydson Simões dos Reis [a], Santosh Govind Khokarale [b], Simon Ekman [c], Eder C. Lima [d], Shaojun Xiong [a], Malin Hultberg [e]

[a] *Department of Forest Biomaterials and Technology, Swedish University of Agricultural Sciences, Umeå SE-901 83, Sweden*
[b] *Technical Chemistry, Department of Chemistry, Chemical-Biological Center, Umeå University, SE 901 87 Umeå, Sweden*
[c] *Department of Applied Physics and Electronics, Umeå University, Umeå SE 901 87, Sweden*
[d] *Federal University of Rio Grande do Sul, Porto Alegre, Brazil*
[e] *Department of Biosystems and Technology, Swedish University of Agricultural Sciences, Alnarp SE 230 53, Sweden*

ARTICLE INFO

ABSTRACT

Edible white-rot mushrooms are organisms that are cultivated at an industrial scale using wood-based substrates. The mushroom industry has an estimated annual production of 34 Mt of edible mushrooms, and approximately 70 wt% of the substrate is left as waste known as spent mushroom substrate (SMS). The huge volumes of SMS generated by mushroom farms hinder proper recycling, meaning that combustion or open-field burning are common disposal practices. This paper shows a concept that could help reduce the environmental impact of the mushroom industry. SMS from the cultivation of shiitake mushroom was used as a carbon precursor for the production of nitrogen-doped activated biochar that was used to remove reactive orange-16 (RO-16) azo dye from water, as well as contaminants from two synthetic effluents and real sewage water. Melamine was used as a nitrogen dopant and phosphoric acid as an activating agent. Samples without the addition of melamine were used for comparison. The doping/impregnation process was carried out in one-step, followed by pyrolysis at 700 and 900 °C for 1 h. BET, Raman spectroscopy, X-ray photoelectron spectroscopy (XPS) and scanning electron microscopy (SEM) were used for the characterization of the biochars. The specific surface area of the doped samples was slightly lower, i.e., 1011 m^2/g (SMS-700 °C), 810 m^2/g (SMS-700 °C + N), 1095 m^2/g (SMS-900 °C), and 943 m^2/g (SMS-900 °C + N). Raman spectroscopic analysis showed that the N-doped biochars had more defective carbon structures than the non-doped ones. XPS analysis showed that doping with melamine led to the formation of N-functionalities on the surface of the biochar particles. The kinetics of adsorption were well represented by the Avrami model. The adsorption isotherms were well-fitted by the Liu model. The maximum adsorption capacities (q_{max}) of RO-16 were much higher for the N-doped biochars, i.e., 120 mg/g (SMS-700 °C), 216 mg/g (SMS-700 °C + N), 168 mg/g (SMS-900 °C), and 393 mg/g (SMS-900 °C + N). N-doped biochar samples were more effective for the removal of contaminants from synthetic effluents and sewage water. N-doped biochar produced at 900 °C showed good recyclability. This work concludes that SMS is a valuable waste that could be used for the production of activated carbon and that N-doping helped to improve the adsorption performance to a great extent.

1. Introduction

According to statistics, only in the EU the present availability of cellulosic biomass residues is 225 Mtonnes/yr, and the projected amount by 2030 is 223 Mtonnes/yr [1]. These wastes include low-quality biomasses from the paper, timber, food, agricultural and forestry industries, and in most countries, incineration and landfilling are used as the main routes of disposal. Wastes such as these do not need to be seen as a disposal problem but as a sizable opportunity to produce sustainably added-value products that could help to reduce the

environmental impact associated with their elimination [2]. White-rot mushrooms are organisms that are cultivated on substrates made of lignocellulosic materials. They secrete different types of enzymes that allow them to use lignin, cellulose and hemicellulose as carbon sources. Cultivation of these types of mushrooms has been done for hundreds of years for food and traditional medicine purposes. The estimated world annual production of edible mushrooms is approximately 34 Mtonnes, with a 30-fold increase since 1978 [3]. In well-managed mushroom industries, after harvest of the mushroom fruit bodies, around 70 wt% of the substrate is left as a waste known as spent mushroom substrate (SMS) that today has no commercial value and is usually used as fuel [4], but could be used for better purposes such as the production of carbon-based adsorbents for water treatment. The degradation of lignin and hemicellulose caused by this type of mushroom is usually larger compared to cellulose [5], and this can give SMS some advantages compared to regular biomasses.

Today's rising advances in civilization lead to an ever-increasing need for effective technology to remove harmful contaminants from wastewater as well as water abstracted for human consumption. Dyes and pigments are colourants that are widely used in the textile, leather, paper and plastic industries, and represent a group of chemicals that can cause serious problems when they come in contact with aquatic ecosystems [6]. Among colourants, reactive azo dyes are a group of synthetic chemicals that are chiefly used in the textile industry, which is among the anthropogenic activities that most use and pollute water [7]. Studies have found that a large amount of the dyes used in dying processes end up in wastewater [8], which in countries with poor environmental legislation is discharged into rivers that are sometimes used for irrigation in agriculture. Under natural environmental conditions, azo dyes do not degrade, and when dye-loaded wastewater is released into the environment affects the entire ecosystem [9,10]. The presence of azo dyes in the soil has negative effects on seed germination and root development of plants as well as microbial communities [11]. In developing countries is also common that drinking water sources are affected by industrial activities [12], and research has shown that water-soluble azo dyes can cause bladder and liver cancers in humans [13,14].

The most effective methods to remove water-soluble pollutants from water, even at very low concentrations, are based on adsorption with materials such as activated carbon. The latter is commonly made using biomass wastes such as coconut shells [15], fruit stones [16], and wood sawdust [17], among others. The processes by which organic pollutants are removed by the activated carbon are usually associated with pore-filling, van der Walls forces, and surface functionalities. In recent years, research work has implemented the concept of heteroatom doping to broaden the spectrum of biochar applications. Doping processes with elements such as nitrogen (N) are among the most used; however, the influence of nitrogen functionalities on the removal of azo dyes from aqueous solution has been comparatively little studied. Among works published in the literature are those from Liu et al. [18], who studied N-autodoped carbons developed from fish waste that were found to be effective adsorbents for the removal of acid orange-7; and Peng et al. [19], who studied the effect of N-doping of ordered mesoporous carbons on the adsorption of acid black-1. In principle, the process is based on the incorporation of functional groups attached to the carbon framework, which change the surface chemical properties and improve the adsorption performance.

This paper focuses on the characterization of nitrogen-doped activated biochars produced using SMS from the cultivation of shiitake mushrooms. SMS samples were doped with melamine ($C_3H_6N_6$), and phosphoric acid (H_3PO_4) was used as a chemical activator to generate a porous carbon matrix. Activated doped biochars were produced by pyrolysis at 700 °C and 900 °C. The carbons were characterized using X-ray photoelectron spectroscopy (*XPS*), Raman spectroscopy, and surface area analysis (BET). The effectivity of the N-doped activated carbons to remove azo dyes from aqueous media was determined using reactive orange-16. The efficiency of the carbons to remove contaminants in

realistic conditions was tested using synthetic effluents and sewage water that was obtained from a communal wastewater treatment plant located in northern Sweden.

2. Materials and methods

2.1. Raw materials

Spent mushroom substrate (SMS) from the cultivation of shiitake (Lentinula edodes) was obtained from previous work [20]. The SMS used here was based on alder wood (*Alnus incana* [L.] Moench) sawdust used as the main raw material for growing the mushroom. Blocks of SMS were ground using a hammer mill and sieved afterwards. A fraction with a particle size of 2–3 mm was chosen as carbon precursor. Melamine (99.9 %, Sigma-Aldrich) was used as a nitrogen-dopant and phosphoric acid (50 % water solution, Merck KGaA, Germany) as a chemical activator. Reactive orange-16 (RO-16) from Sigma-Aldrich was used as a model azo dye for adsorption experiments.

2.2. Doping and activation process

The doping and impregnation process was carried out in one step. The precursor, N-dopant and P-chemical activator were mixed using a weight ratio of 1 SMS: 0.5 melamine: 5 H_3PO_4. Samples made using a weight ratio of 1 SMS: 5 H_3PO_4 were used for comparison. The mixtures were kneaded to obtain a homogeneous paste and let soak for 6 h at ambient temperature. Afterwards, the samples were dried at 60 °C for 15 h. Next, samples were pyrolysed at 700 °C and 900 °C using a stainless steel reactor heated externally by a muffle furnace (Carbolite Gero ELF 11/14). The temperature of the reactor was increased from room temperature to the final treatment temperature at a heating rate of 10 °C/min and kept for 1 h. Nitrogen gas was used to keep an inert atmosphere during pyrolysis. After the treatment, the furnace was turned off and the samples were allowed to cool down to room temperature. The resulting biochars were washed with boiling distilled water until neutral pH and finally dried in an oven at 105 °C overnight.

2.3. Characterization of the activated biochars

The textural characterization of the samples was carried out using a Tristar 3000 sorptometer (Micrometrics Instrument Corp., Norcross, GA, USA). The Brunauer-Emmett-Teller (BET) principle was used to calculate the specific surface area (SSA) of the samples, and the Barrett-Joyner-Halenda (BJH) model was used to obtain the pore volume and pore size distribution. The sample's graphitization degree was calculated from their Raman spectra, measured using a Bruker Bravo spectrometer (Bruker, Ettlingen, Germany). Samples were ground using an agate mortar and pestle and then scanned in the 300–3200 cm^{-1} spectral range. The spectra were processed in OPUS (version 7) by baseline correction (64-point rubberband), smoothing (13-point) and vector normalisation in the range 350–2100 cm^{-1}. Surface functionalities were identified by X-ray photoelectron spectroscopy (XPS) analysis. The spectra were obtained using a Kratos Axis Ultra DLD device equipped with an Al K_α X-ray source operated at 150 W. Survey spectra were obtained at a pass energy of 160 eV, and individual photoelectron lines were acquired at 20 eV. The value for the point of zero charge (pH_{pzc}) of each biochar was obtained by plotting the measured zeta potential value with the pH measured via a Zetasizer Nano ZSE 3700 (Malvern Instrument Co., Malvern, UK) at 22 °C varying the pH from 2 to 10.

2.4. Bach adsorption experiments and regeneration studies

All the carbons used for adsorption experiments had an average particle size of 1–2 mm. Adsorption experiments were performed using RO-16 aqueous solutions with concentrations of 30–1200 mg/L. The effect of the adsorbent dosage was measured by contacting dye solution

(100 mg/L, pH 6) with adsorbent doses of 0.5 to 5 g/L. The solutions containing the adsorbent were agitated at 22 °C for 5 h using an orbital shaker (IKA KS250). Afterwards, the solutions were left to rest for 5 min to let the carbon particles precipitate. The residual concentration of the dye in the solution was quantified by UV–Vis spectrophotometry using a Shimadzu 1800 device at a λ_{max} of 494 nm calibrated using standard dye solutions.

The effect that the pH of the dye solution has on the removal capacity of the biochars was determined at room temperature using dye solutions with a concentration of 100 mg/L and pH ranging from 2 to 10 that were contacted with 1 g/L of each biochar. The pH of the solutions was adjusted with HCl or NaOH. Solutions containing the biochar samples were agitated for 5 h, after that the biochar was separated and quantification of the amount of dye removed was carried out as previously described.

Kinetic studies were performed at room temperature using a carbon dose of 1 g/L and a dye solution with a concentration of 100 mg/L and pH 6. The amount of the dye removed from the solution by the carbon was measured periodically between contact times of 1 and 480 min using the procedure previously described.

Equilibrium isotherm measurements were carried out at room temperature by contacting each biochar (1 g/L) with solutions of RO-16 (30–1200 mg/L, pH 6). The samples were agitated for the time needed to reach the equilibrium as was previously determined in the kinetic measurements. The amount of the dye remaining in the solution was determined as already described.

The amount of the dye removed from the solution (Eq. (1)) expressed as q (mg/g), and the percentage of removal (Eq. (2)) expressed in per cent, were used to quantify the adsorption performance.

$$q_e = \frac{C_i - C_e}{m} * V \qquad (1)$$

$$Removal\left(\%\right) = 100 * \frac{C_i - C_e}{C_i} \qquad (2)$$

where, q_e is the dye adsorption capacity expressed in mg dye/g adsorbent, C_i and C_e are the initial and final concentrations of the dye in the solution expressed in mg/L, V is the volume of the dye solution used in each measurement expressed in L, and m is the mass of the biochar sample expressed in grams.

For regeneration studies, biochar samples were first saturated with RO-16 and then washed with water to remove any unadsorbed dye. Then, the saturated samples were dried overnight in an oven at 70 °C. Since this dye shows its highest adsorption capacity under acidic conditions, a basic eluent, i.e., 0.25 M NaOH +20 % EtOH, was used. The saturated and dried biochars were put in contact with the eluent and then agitated for 4 h to promote the liberation of the adsorbed RO-16 molecules. The desorbed RO-16 was separated from the biochar by centrifugation. Again, the biochars were washed with water to remove the eluent and dried overnight in an oven at 70 °C. This procedure was repeated until five cycles were completed. The adsorption capacity (q) was measured at each cycle.

Experiments mentioned above were carried out 3 times, and average values with standard deviation are reported.

2.5. Removal of contaminants from synthetic effluents and real sewage water

The produced N-doped and non-doped biochars were tested for their ability to remove contaminants from water in realistic conditions. Laboratory-made aqueous effluents (Table 1) made of different dyes and inorganic compounds, as well as real sewage water were used for this characterization. The sewage water was obtained from a wastewater treatment plant located in Umeå, Sweden. The plant uses mechanical, biological and chemical processes to treat wastewater that comes mainly

Table 1
Effluent compositions and concentrations.

Compounds	Concentration (mg/L)		λ_{max} (nm)
	Effluent-A	Effluent-B	
Acid red-18	50	50	507
Reactive orange-16	50	50	494
Reactive blue-4	50	50	595
Methylene blue	50	50	668
Evans blue	50	50	468
Phenol red	50	50	550
Crystal violet	50	–	590
Methyl red	50	–	507
Bismarck Brown	–	50	468
Methyl orange	–	50	522
Sodium dodecyl sulphate	25	25	–
Sodium sulphate	25	25	–
Ammonium chloride	20	25	–
Sodium acetate	20	25	–
pH	5.4	5.2	–

from households. Raw sewage water was collected after the mechanical treatment where all kinds of insoluble coarse materials were removed. The treated sewage water was collected after the chemical treatment where iron chloride flocculant was used to remove all kinds of solid particles before the water was returned to a river nearby the facility. Both the raw and the treated sewage water samples were filtered before adsorption experiments to remove solid particles that interfered with the measurements.

The total amount of contaminants removed by each biochar was determined based on the integrated area under the UV–Vis 190–800 nm spectral range of the tested adsorbates before and after the treatment with the biochars. The area under the spectra was calculated using the OriginPro 2020 software.

3. Results and discussion

3.1. Textural analysis of the produced activated biochars

The N$_2$ isotherms for the activated biochar samples (Fig. 1) can be classified as type IV, according to IUPAC classification [21]. Type IV isotherms exhibit a hysteresis loop suggesting a high presence of mesopores [22,23]. However, the high N$_2$ uptake at low partial pressure suggests the presence of microporous features in the carbon structure. What is observed in N$_2$ curves is corroborated by the pore size distribution curves of the carbons shown in Fig. 1. The porous carbon structure is composed of a fraction of pores with diameters of up to 2 nm (micropores) and a big fraction of less than 5 nm (small mesopores). Non-doped samples exhibited fractions with bigger mesopores compared to the doped materials. It seems that the melamine doping created smaller mesopores compared to the non-doped samples. Such differences in pore size distribution in the prepared carbons could lead to better adsorptive properties. To further evaluate the porosity features of the materials, the BET surface areas were accessed (Table 2). The results show that the SSA of both biochars was high; however, the melamine doping provoked a small reduction in BET surface areas at both pyrolysis temperatures. The same trend was observed in other works dealing with N-doping of similar precursors [24]. The areas obtained by the authors were 1086 and 1003 m^2/g, for non-doped and nitrogen-doped biochars, respectively.

3.2. Scanning electron microscopy (SEM) analysis

SEM was used to observe the effect of temperature and melamine doping on the biochars' morphologies. The micrographs corresponding to the biochars' surface at 5 K of magnification are shown in Fig. 2. The SEM images show that both temperature and melamine doping yielded carbon materials' surfaces with different features. The sample SMS-
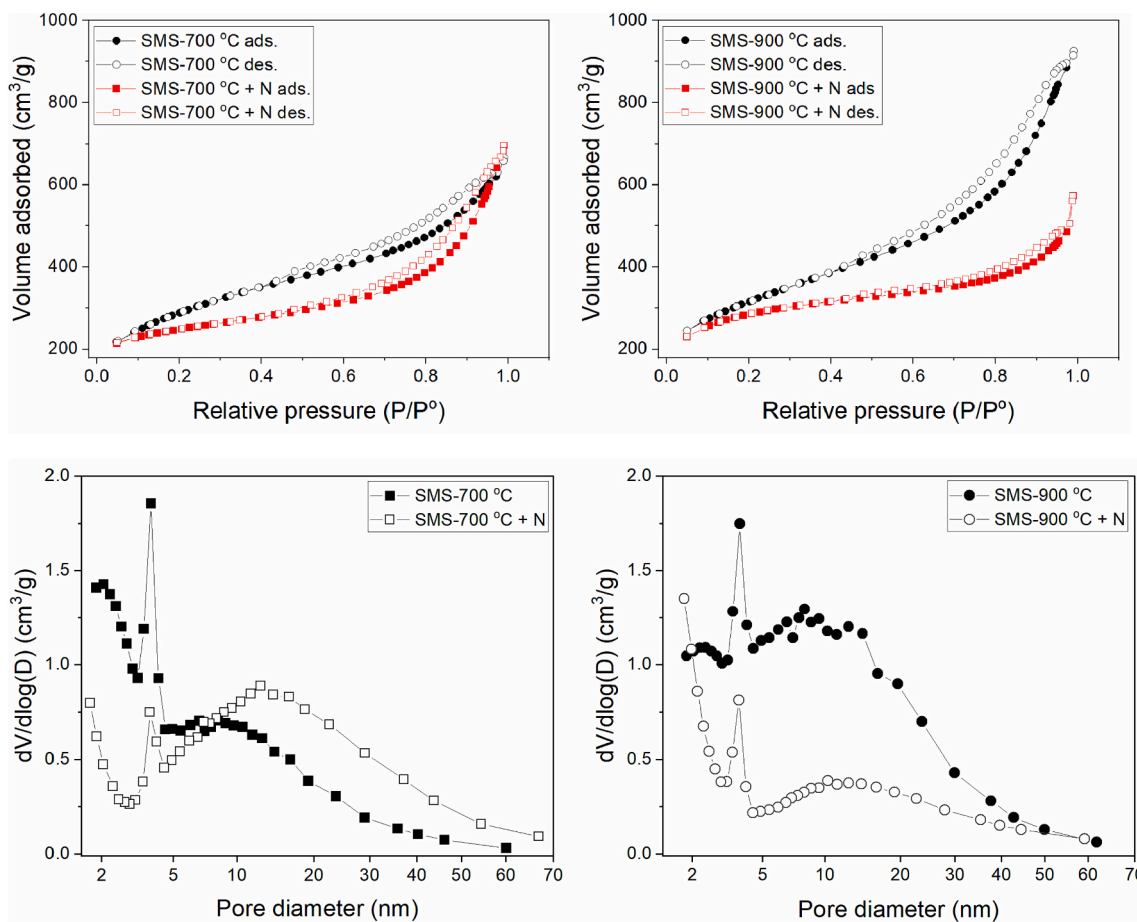
Fig. 1. N$_2$ adsorption isotherm and pore size distribution for the N-doped and non-doped biochars.

Table 2
Textural properties of the N-doped and non-doped biochars.

	SMS-700 °C	SMS-700 °C + N	SMS-900 °C	SMS-900 °C + N
Surface area				
BET SSA (m^2/g)	1011	810	1095	943
Micropore area (m^2/g)	117	412	181	372
Micropore area (%)	12	51	16	39
Mesopore area (m^2/g)	893	398	915	571
Mesopore area (%)	88	49	84	61
Pore volume				
Total pore volume (cm^3/g)	1.03	1.08	1.43	0.89
Micropore volume (cm^3/g)	0.05	0.21	0.09	0.19
Micropore volume (%)	5	19	6	21
Mesopore volume (cm^3/g)	0.98	0.87	1.34	0.70
Mesopore volume (%)	95	81	94	79
Pore size				
Average pore width (nm)	4.08	5.31	5.23	3.76

700 °C presented a less rough surface but with several small pores (highlighted in the red rectangular shapes, Fig. 2a). The doped biochar pyrolysed at 700 °C (SMS-700 °C + N) presented a much rougher surface compared to the non-doped (SMS-700 °C), what can be related to the effect of melamine doping that created more physical defects and

micropores on the biochar. The same behaviour was observed in the biochars pyrolysed at 900 °C. The sample SMS-900 °C exhibited a very rough but cohesive surface while SMS-900 °C + N exhibited a more defective morphology. Carbon materials rich in defects are reported to be suitable adsorbent materials because the defects can act as adsorptive sites [24,25].

3.3. Raman spectra

Raman spectroscopy is considered one of the most informative methods for evaluating the structural perfection and degree of order/graphitization of bio-based carbon materials. The Raman spectra of each non-doped and N-doped biochar (Fig. 3) show the D-peak that arises due to the broken symmetry of the hexagonal structure of the carbon atoms. Defects in the lattice are caused by the asymmetry, also due to the carbon atom sp^3 hybrid configuration, represented by a disordered and amorphous defective structure. The second peak at around 1600 cm^{-1} (G-peak) is characteristic of carbon atom sp^2 hybrid configuration, related to the crystalline graphite structure. The area ratio between the D and G peaks (A$_D$/A$_G$) gives information about the level of order/disorder, also called the degree of graphitization, of the carbon structure. As is shown in Fig. 3, the doping process led to an increase in the A$_D$/A$_G$ ratio at both pyrolysis temperatures, meaning that the structure of the carbon matrix in doped carbons contains a larger amount of defects, which is corroborated by the SEM analysis (Fig. 2). Carbons with defective structures can lead to better adsorption performance [2,24].

3.4. X-ray photoelectron analysis

XPS analysis was performed to identify the elements present at the
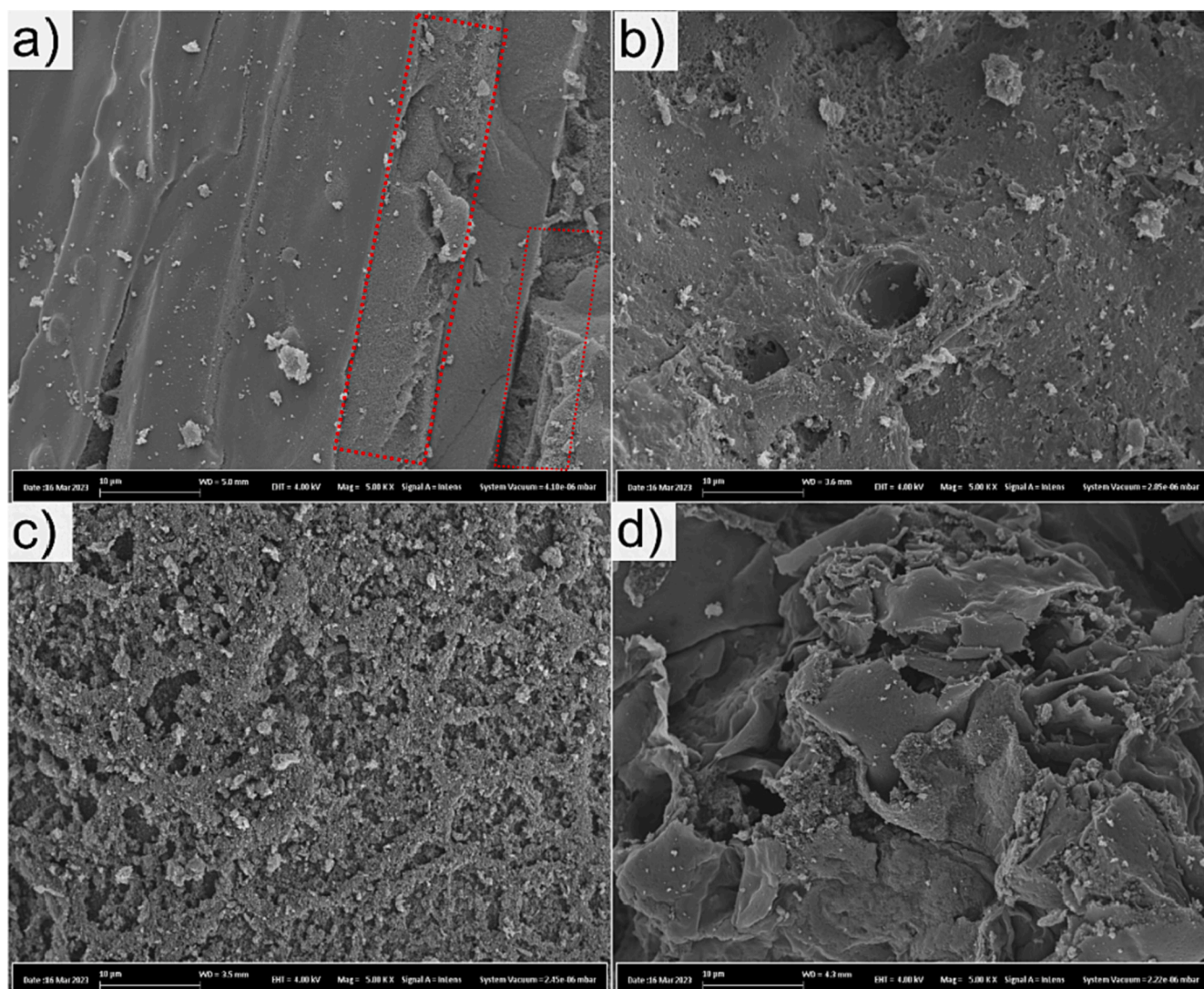
Fig. 2. SEM images of the SMS-700 °C (a), SMS-700 °C + N (b), SMS-900 °C (c), and SMS-900 °C + N (d) at a magnification of 5 kX.

surface of the biochars, as well as their chemical state. Only the biochars produced at a pyrolysis temperature of 900 °C were subjected to the XPS analysis due to their better performance in the adsorption tests (see following sections). The survey spectra and atomic concentrations of all elements found at the surface of the biochars are given in Fig. 4 (a, b) and Table 3, respectively. XPS analysis revealed the presence of C, O, N, and P on the surface of both non-doped and N-doped biochars. The non-doped sample had also small amounts of Fe and Cr, which are contaminants from the reactor used for pyrolysis. The content of N in the N-doped biochar was more than 3 times higher than in the non-doped.

The N 1s spectra are presented in Fig. 4 (c, d). The signal of the non-doped biochar was decomposed into two forms of nitrogen, and that of the N-doped biochar was decomposed into five. The non-doped biochar presented two main peaks at 399.1 and 401.3 eV, related to pyrrolic-N and graphitic-N states. On the other hand, the N-doped biochar (SMS-900 °C + N), presented five main peaks highlighting the effectiveness of the N-doping in introducing N atoms in the biochar structure. The five peaks are at 398.2 eV (pyridine-N), 399.5 eV (pyrrolic-N), 400.9 eV (graphitic-N), 402.5 eV (C-NH$_2^+$), and 405.4 eV (oxidized-N), respectively. This demonstrates that the doping with melamine led to the formation of N-functionalities on the surface of the biochar particles that may play an important role in the removal of contaminants from aqueous solutions.

3.5. Effect of the adsorbent dose on RO-16 removal

The study of the effect of adsorbent dosage in any adsorption process is an important step to evaluate the efficiency and suitability/applicability of the adsorption process on a real industrial scale. Fig. 5 shows the effect of biochars' doses (ranging from 0.5 to 5 g/L) on RO-16 (C$_o$ of 100 mg/L) removal by non-doped and N-doped biochars.

The curves show that the doped biochars led to much better results with a lower amount of adsorbent dose compared to the non-doped. For instance, for the biochars prepared at 700 °C, the non-doped reached 54 % with 2 g/L of biochar, while N-doped reached 90 % with the same dose (2 g/L). The samples made at 900 °C had even better results; employing 2 g/L, the non-doped removed 76 % of the RO-16, while the N-doped carbon (SMS-900 °C + N) removed 100 %. One can see that the amount of dye removed from the solution does not follow the surface area of the biochars (Table 2), meaning that the surface functionalities created on the carbon surface during the doping process played an important role in the adsorption mechanism.

Although 2 g/L was shown to be the most effective dose (based on SMS-900 °C + N results), for the following experiments a mass of 1 g/L was selected. At 1 g/L a dye removal of 72 % was achieved (with a q equal to 72 mg/g) (see Fig. 5b), compared to 2 g/L which gives a dye removal of 100 % and a q equal to approximately 50 mg/g. Using 1 g/L instead of 2 g/L leads to a reduction in the amount of used adsorbent of
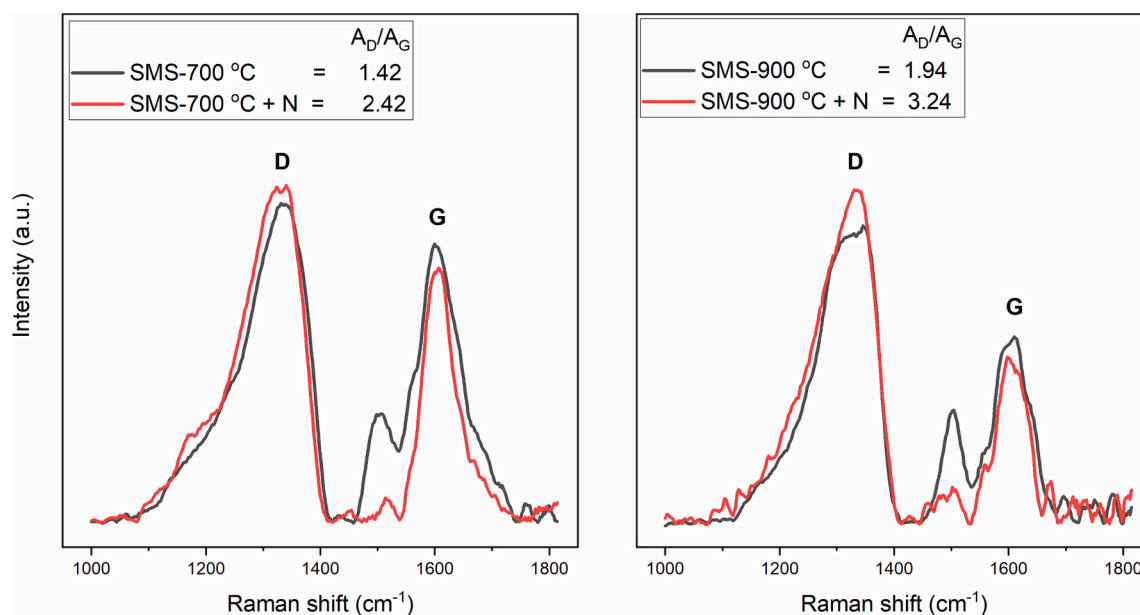
Fig. 3. Raman spectra of the N-doped and non-doped biochars.

50 % and an increase of approximately 30 % in the q. In summary, increasing the adsorbent amount is not justified economically speaking.

3.6. Point of zero charge (pH_{pzc}) and effect of pH

The pH_{pzc} is an important measurement for the determination of the charge of an adsorbent, which helps to understand the interaction between adsorbent and adsorbate. Only the biochar samples pyrolysed at 900 °C were analysed here due to their better RO-16 adsorption performance. The pH_{pzc} of the SMS-900 °C and SMS-900 °C + N biochars was performed to understand the effect of the N-doping on the biochar's surface properties. The pH_{pzc} indicates the point where the biochar's surface potential is equal to zero, but also that for values below pH_{pzc}, the biochar surface is positively charged, and above will be negatively charged [28,29]. The effect of N-doping on surface zeta potentials of the biochars in relation to the pH of solution are compared in Fig. 6a. The pH_{pzc} of SMS-900 °C + N sample was 4.7, being higher than that of the non-doped sample (SMS-900 °C, $pH_{pzc} = 3.7$). The doping of biochar with nitrogen due to its low electronegativity (3.04) compared to oxygen (3.44), affects biochar surface chemistry and isoelectric point. pH's < pH_{pzc} would be favourable for the RO-16 anionic dye adsorption. This suggests that the nitrogen-doped sample (SMS-900 °C + N) is positively charged at pH below 4.7, which favours the removal of anionic RO-16 [30].

Together with pH_{pzc}, the pH of the solution also has a huge impact on the removal of dyes because it influences both adsorbent-adsorbate charges and their abilities to bind through electrostatic interactions. Only the biochar samples pyrolysed at 900 °C were analysed due to their better RO-16 adsorption performance. Fig. 6b shows the results of the RO-16 adsorption capacity measurements at pH's from 2 to 10.

The removal of RO-16 was highest at pH 2.0; at pH < pH_{pzc}, the RO-16 anionic dye adsorption is facilitated when the concentration of proton is high, and it decreases with the increased pH due to the protonation of amino groups on the surface of the biochars [31,32]. Literature shows that anionic dyes, such as RO-16, have their uptake rate increased at lower pH, mainly due to the electrostatic interactions [33]. In acid conditions, probably, the van der Waals interactions and H-bonding become dominant in the adsorption mechanism [34].

Since in normal cases, effluents such as sewage water and similar have a pH that is around 5 to 8, the kinetic and equilibrium measurements in the following sections were made at the natural pH of deionised water, i.e., 6.

3.7. Kinetics of RO-16 adsorption on the biochars

The adsorption kinetics gives important information to understand the processes by which the contaminant in the solution is removed by the adsorbent. The non-linear pseudo-first order (PFO), pseudo-second order (PSO) and Avrami-fractional order (AFO) kinetic models were applied to the experimental measurements [35,36]. The models' suitability was statistically evaluated through R^2_{adj} and SD values. Mathematical expressions are given in the supporting information. The model that presents the best fitting to the experimentally measured points has the smaller SD and the higher R^2_{adj} values, which statistically suggest a smaller disparity between experimental and theoretical q values given by the models.

The kinetic measurements and parameters from each model are shown in Fig. 7 and Table 4, respectively. The same trend was observed for all adsorbents, a fast uptake RO-16 amount within 60 min, followed by a slow increase until equilibrium is achieved at approximately 200 min. According to the parameters obtained from each model (Table 4), the AFO showed to be the most adequate to describe the experimental results for all carbons. AFO is a widely employed model to study the kinetics of the adsorption process and its suitability means a highly complex kinetic adsorption process with several pathways and mechanisms [37,38].

The intra-particle diffusion process was accessed to further study the kinetic process regarding the influence of mass transfer. The curves show that the adsorptive process involving the biochars and RO-16 possesses three stages (see Fig. 7 c, f). The first stage is the longest for all carbons and this stage is attributed to the RO-16 molecule's transport towards biochar adsorbent surfaces [39]. Since the biochars are highly porous with very high surface area, it is reasonable that this first stage takes a longer time. In addition, the doped biochar presented a first stage longer than the non-doped, which can be due to the higher number of active sites introduced by the nitrogen doping that can offer high resistance to liquid permeation [40]. The second stage is a fast process and it can be related to intra-particle diffusion [39]. The biochars are rich in pores larger than the RO-16 molecule and this can justify the faster diffusion of the dye molecules into the porous adsorbent. The third stage can be related to the final equilibrium stage, in which the intra-particle diffusion slows down due to the low RO-16 concentration in
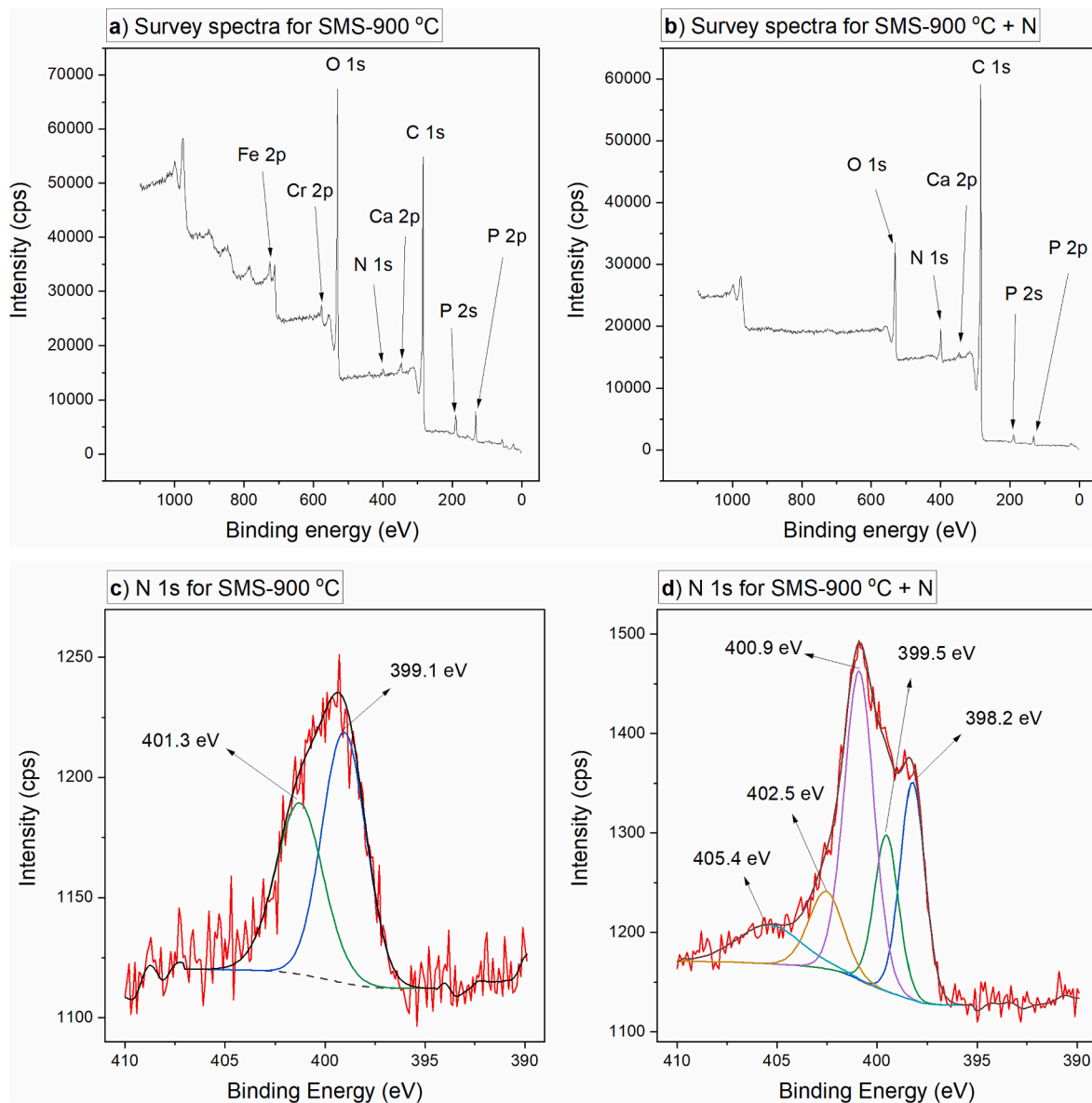
Fig. 4. XPS survey spectra (a, b) and deconvoluted N 1s peaks (c, d) of the N-doped and non-doped biochars produced at 900 °C.

the liquid and the further diffusion of RO-16 into the very small pores until the equilibrium is reached [41]. The intra-particle kinetic curves show three well-defined linear stages, which indicate that the adsorption of RO-16 on the biochars is controlled by the resistance mass transfer [39].

The contact time for subsequent RO-16 adsorption tests was set at 6 h (360 min) to ensure that the contact time was sufficient for attaining equilibrium.

3.8. Equilibrium isotherms of RO-16 adsorption

Equilibrium isotherms are widely employed to understand the adsorption process and interaction between the adsorbate and the adsorbent. In this work, three isotherm models including Langmuir, Freundlich, and Liu, were employed to understand the adsorption of RO-16 by the biochars. The mathematical expressions of each model are given in the supporting information.

The equilibrium curves and the parameters obtained from each model are shown in Fig. 8 and Table 5, respectively. The R^2_{adj} and SD values were used to judge the suitability of the models. Thus, Liu gave

the lowest SD and highest R^2_{adj} values for all four biochars (non-doped and N-doped), which means that it is the most suitable model for describing the equilibrium isotherms for RO-16. It also means that the maximum adsorption capacity values obtained from the Liu model were closer to those found experimentally. The maximum RO-16 adsorption capacity for the N-doped biochars was higher than that of the non-doped (Table 5). The Langmuir and Liu models possess lower SD and higher R^2_{adj} when compared to the Freundlich model, suggesting that the adsorption of RO-16 on biochars prepared in this work has a more homogeneous characteristic on monolayers than a heterogeneous process [42,43].

3.9. Comparison of biochars q_{max} with other adsorbents in the literature data

Table 6 compares the maximum RO-16 adsorption capacity (q_{max}) obtained in this work to literature values for different types of adsorbents. The q_{max} of the SMS-900 + N is among the best performances compared to the other adsorbents. In the work of Abdulhameed et al. [44], chitosan-tripolyphosphate/titanium dioxide nanocomposites were

Table 3
XPS surface elemental analysis of the non-doped and N-doped biochars produced at 900 °C.

Element	SMS-900 °C (at.%)	SMS-900 °C + N (at.%)	Nitrogen state	Forms of nitrogen	Reference
C	69.4	84.1			
O	25.5	10.8			
N	1.3	4.1			
P	3.8	1.3			
Ca	0.4	0.2			
Fe	2.4	Traces			
Cr	0.6	No			
C/N	53.4/1	20.5/1			
N 1s peaks BE (eV)					
398.2		0.89		Pyridinic nitrogen	
399.1–399.5	0.75	0.73	C–N–C	Pyrrolic nitrogen	[26,27]
400.9–401.3	0.57	1.53	C–N$^+$H–C	Graphitic nitrogen	[26,27]
402.5		0.44	C–NH$_2^+$		
405.4		0.51	NO$_2$	Oxidized nitrogen	[26,27]

used for the removal of RO-16 from water, and a q_{max} value of 618.7 mg/g was obtained. Although this adsorbent presented a higher q_{max} value than the SMS-900 + N biochar (392.9 mg/g), its synthesis cost is higher than the biochars produced in this work using waste from the mushroom industry (SMS). Thus, taking into consideration the adsorbent production cost, N-doped SMS-based carbons can be seen as an effective and cheap option for the treatment of dye-polluted water.

3.10. Mechanisms of adsorption

Based on the results obtained from the characterization of the biochars and adsorption tests, a possible adsorption mechanism can be proposed (Fig. S1 in supporting information). The removal of the dye from the solution was achieved by a combination of physical interactions, known as pore filling, which is related to the specific surface area of the adsorbent, together with other mechanisms such as chemical interactions including electrostatic, hydrogen bonding, π-π and Lewis acid-base interactions [31–34]. Since the specific surface area of the biochars was high, physical adsorption was probably the main

contributor to the removal of the dye from the solution. However, even if the specific surface area of the non-doped activated biochars was higher than the N-doped ones (Table 2), the N-doped biochars resulted in a much higher maximum adsorption capacity (Table 5). This means that the surface functionalities introduced by the dopant agent (melamine), as shown by the XPS analysis (Fig. 4 and Table 3), probably increase the electrostatic interactions between the adsorbent and the RO-16 dye, which in turn improved the adsorption performance. In summary, the doping process with melamine on the carbon matrix probably contributed to forming a positive charge on the surface of the biochar that increase the electrostatic attraction with negatively charged –SO$_3^-$ groups of the RO-16 molecule leading to an improvement in the adsorption performance.

3.11. Treatments of synthetic effluents and sewage water

So far, the adsorption results proved that the prepared biochars exhibited remarkable efficiency in removing a single dye (RO-16) from aqueous solution. Thus, the applicability of the biochars in treating synthetic wastewaters (made of several dyes and inorganic compounds, Table 1), as well as raw and treated sewage water collected from a communal sewage water treatment plant was accessed.

The UV–Vis absorption spectra 190 to 800 nm before and after the batch-contact adsorption (Fig. 9) were recorded for all biochars. The overall percentage of removal of contaminants from the solution was calculated by integrating the area under the absorption band 199–800 nm.

For the synthetic effluents A and B, the adsorption process was carried out at 22 °C, a pH of approximately 6.0 (slightly acidic), and an adsorbent dosage of 1.0 g/L. For Effluent A, the attained percentages of removal were 54 % (SMS-700 °C), 62 % (SMS-700 °C + N), 56 % (SMS-900 °C), and 68 % (SMS-900 °C + N). For effluent B, the reached percentages of removal were 50 % (SMS-700 °C), 59 % (SMS-700 °C + N), 53 % (SMS-900 °C), and 64 % (SMS-900 °C + N). This shows that the doped biochars had improved outcomes for treating the laboratory-made effluents, following the previous adsorption results made with a single dye.

The raw and treated samples of sewage water were only treated with the biochars produced at 900 °C due to their better performance in previous tests. The types of contaminants present in these samples were previously analysed by Gentili & Fick [53], and Lindberg et al. [54]. Organic matter rich in nitrogen and phosphorus, pharmaceuticals, and
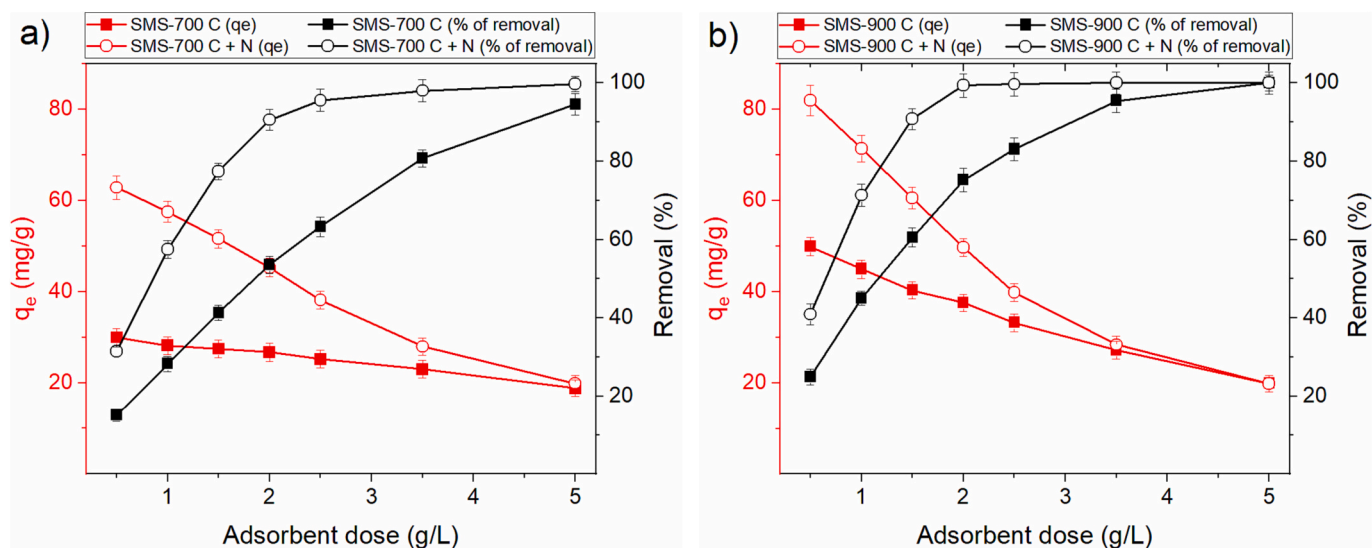

Fig. 5. Effect of the adsorbent dose on the removal of RO-16 for samples pyrolysed at 700 °C (a) and 900 °C (b). Conditions: initial dye concentration = 100 mg/L, pH = 6, temperature = 22 °C.
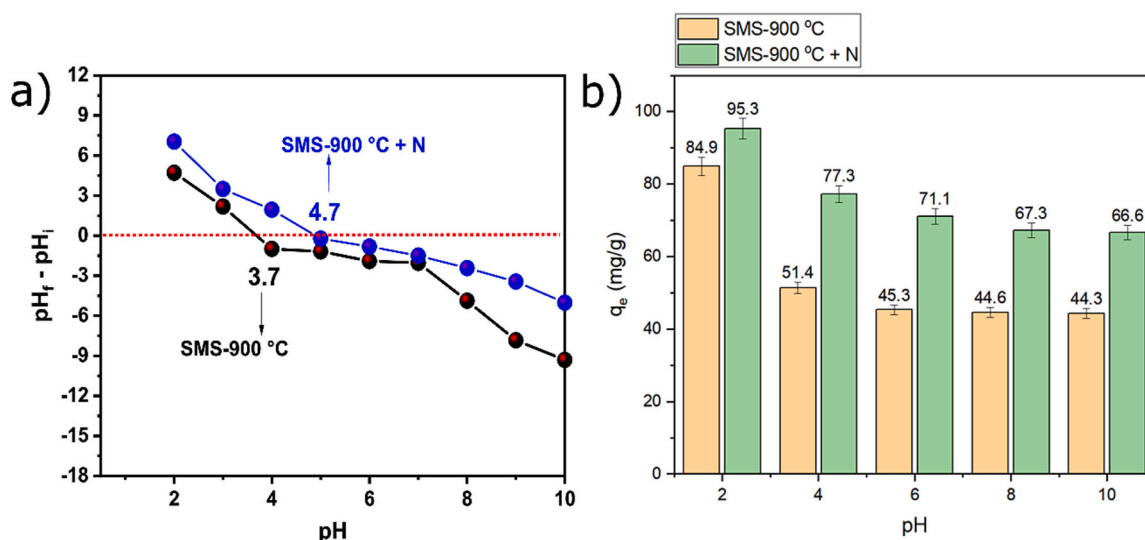
Fig. 6. pHpzc (a) and Effect of the pH (b) on the RO-16 removal onto biochars produced at 900 °C. Experimental conditions: temperature = 22 °C, initial dye concentration = 100 mg/L, contact time = 5 h, dosage of adsorbent = 1 g/L.
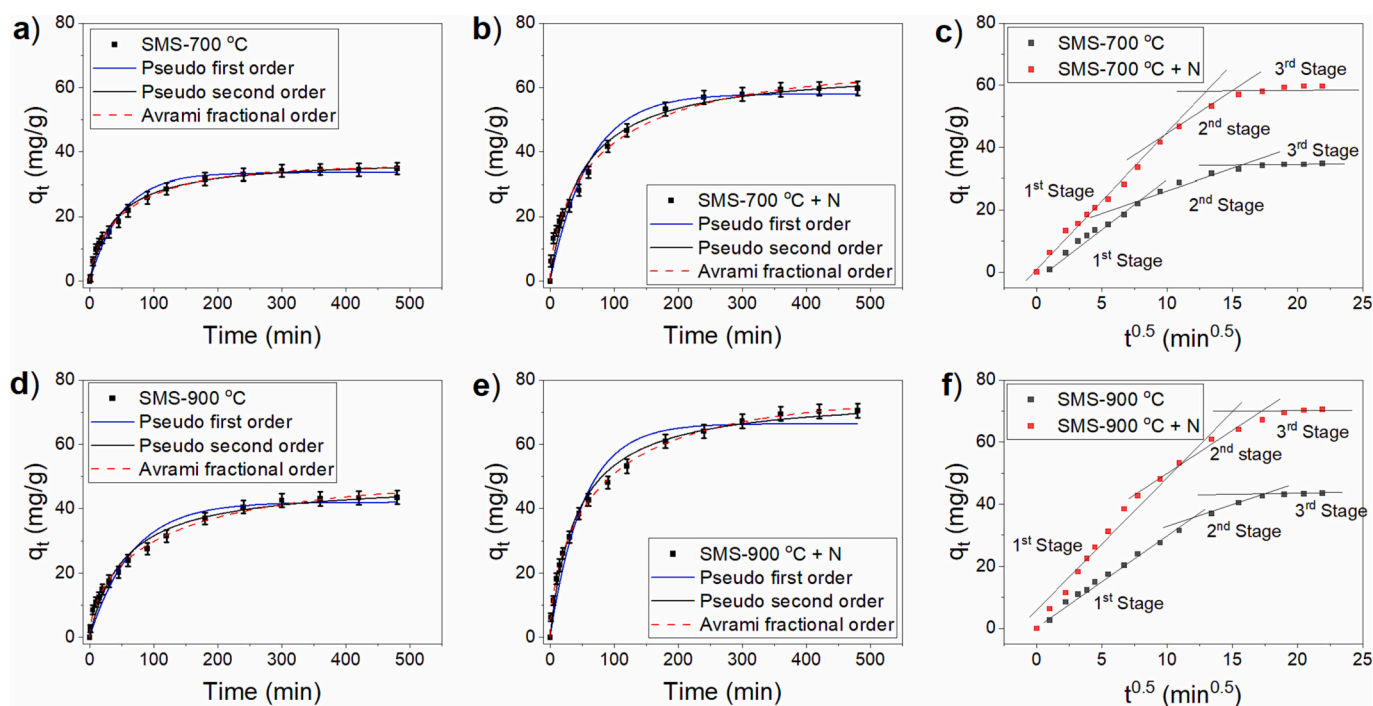

Fig. 7. Reactive orange-16 kinetics of adsorption curves onto SMS-based biochars. Experimental conditions: temperature = 22 °C, initial dye concentration = 100 mg/L, initial pH = 6.0, dosage of adsorbent = 1 g/L.

different salts are the main contaminants in this type of water. The wastewater collected after the treatment works carried out at the plant contained very small amounts of contaminants detectable by UV–Vis analysis. The results show that the percentage of removal of contaminants present in both samples was higher when using the doped biochar. For the raw sewage water, the percentage of removal was 68 % (SMS-900 °C) and 82 % (SMS-900 °C + N). For the treated sewage water, the percentage of removal was 47 % (SMS-900 °C) and 48 % (SMS-900 °C + N), which is reasonable because the treated water contains just traces of organic contaminants, and probably a part of what is present is not detectable by UV–Vis analysis. It is important to highlight that all carbons tested presented satisfactory removal capacity, indicating their good suitability for treating effluents rich in organic and inorganic

contaminants.

3.12. Regeneration studies

The reusability of the adsorbent is important for real-world applications to make the process economically sound. Five adsorption-desorption cycles were carried out. An amount of 50 mg of adsorbent was saturated with a RO-16 solution with a concentration of 500 mg/L (pH 6). Only the biochars that showed the highest adsorption capacity, i. e., SMS-900 °C and SMS-900 °C + N were used for this test. The results from the regeneration tests are shown in Fig. S2 in supporting information.

It was observed that the adsorption capacity of the N-doped and non-

Table 4
Kinetic model parameters for adsorption of reactive orange-16.

	SMS-700 °C	SMS-900 °C	SMS-700 °C + N	SMS-900 °C + N
Pseudo-first-order				
q_e (mg/g)	33.49	41.94	57.95	66.34
k_1 (1/min)	0.0203	0.0152	0.0166	0.0193
R^2_{adj}	0.975	0.961	0.961	0.964
SD (mg/g)	1.928	3.015	4.085	4.552
Pseudo-second-order				
q_e (mg/g)	37.84	48.41	66.39	75.41
k_2 (g/mg min)	6.833 E-4	3.859 E-4	3.111 E-4	3.216 E-4
R^2_{adj}	0.993	0.982	0.978	0.991
SD (mg/g)	1.068	2.035	3.041	2.386
Avrami fractional order				
q_e (mg/g)	35.77	49.63	65.64	75.25
k_a (g/mg min)	0.016	0.0087	0.011	0.0122
n	0.683	0.601	0.618	0.608
R^2_{adj}	0.997	0.996	0.992	0.999
SD (mg/g)	0.652	0.964	1.875	0.688

doped biochars slightly decreased with the regeneration cycles, but they maintained a relatively good adsorption capacity after four cycles. For the SMS-900 °C biochar, the adsorption capacity at the first cycle (131 mg/g) was reduced to 64 mg/g at the end of the fifth cycle. For the SMS-900 °C + N biochar, the adsorption capacity in the first cycle (155 mg/g) was reduced to 85 mg/g in the fifth cycle. These losses of performance during cycling are probably due to mechanical damage of the porous carbon structure or dye molecules sized in small pores. These results indicate that the N-doping process yielded an adsorbent with satisfactory recyclability that could be reused multiple times.

4. Conclusions

Nitrogen-doped activated biochars were developed from hardwood-based spent substrate from the cultivation of shiitake mushrooms. Melamine was used as a dopant and H_3PO_4 as an activation agent. The

Table 5
Equilibrium isotherm model parameters for adsorption of reactive orange -16.

|	SMS-700 °C	SMS-900 °C	SMS-700 °C + N	SMS-900 °C + N
Langmuir				
q_{max} (mg/g)	133.3	145.4	195.2	245.4
K_L (L/min)	0.0064	0.0088	0.0131	0.012
R^2_{adj}	0.987	0.981	0.982	0.976
SD (mg/g)	4.811	6.443	8.954	13.29
Freundlich				
K_F ((mg/g) (mg/L)$_F^{-1/n}$)	8.536	13.49	23.93	31.34
n_F	2.591	2.942	3.251	3.334
R^2_{adj}	0.906	0.957	0.943	0.952
SD (mg/g)	13.03	9.733	15.92	17.76
Liu				
q_{max} (mg/g)	120.4	168.1	216.2	392.9
K_{Li} (L/mg)	0.0081	0.0059	0.0099	0.0024
N_{Li}	1.287	0.764	0.788	0.501
R^2_{adj}	0.993	0.986	0.986	0.979
SD (mg/g)	3.501	5.496	7.914	11.96
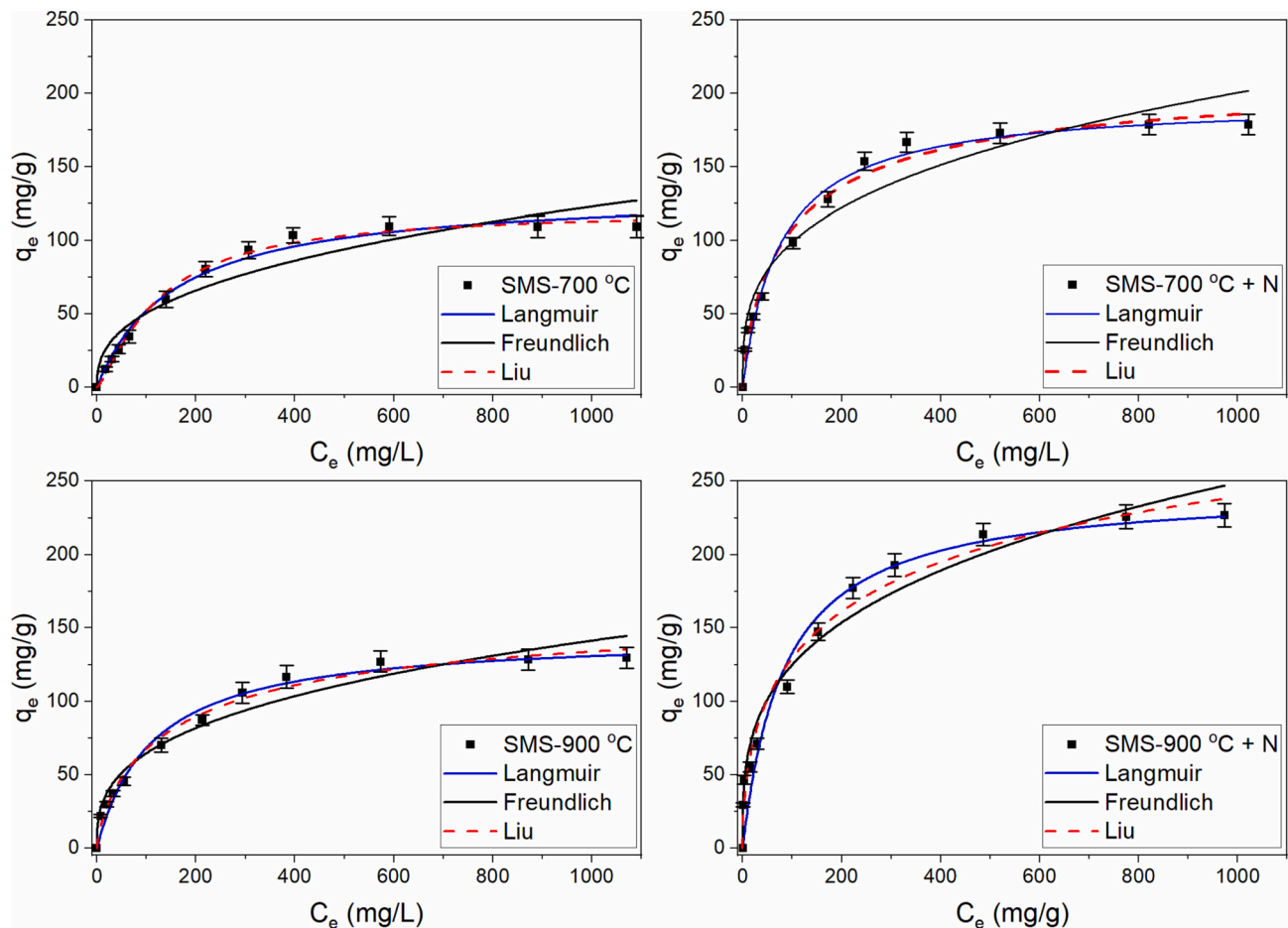
Fig. 8. Reactive orange-16 adsorption equilibrium curves onto SMS-based biochars. Experimental conditions: temperature = 22C, pH 6.0, dosage of adsorbent = 1 g/L, contact time = 6 h.

Table 6

Maximum adsorption capacities (q_{max}) for reactive orange-16 using different adsorbents.

| Adsorbents	S_{BET} (m²/g)	q_{max} (mg/g)	T (°C)	pH	Adsorbent dosage (g/L)	Maximum adsorbate concentration used (mg/L)	Ref.
Chitosan-TPP/TiO₂ nanocomposite	2.75	618.7	40	4.0	4.5	n.d	[44]
Mesoporous carbon from fish scales	213.82	114.2	50	7.0	1	400	[45]
Coffee waste and red mud composite	12.3	144.8	50	2.0	2.5	300	[46]
Paper sludge activated carbon	640	178.0	30	2.0	1	350	[47]
Phyllanthus reticulatus activated carbon	124.7	67.93	30	2.0	1	60	[48]
Chitosan-glyoxal/fly ash/Fe₃O₄ composite	3.31	112.5	40	4.0	1	200	[49]
Landfill sludge biosorbent	n.d	159	25	2	10	5000	[50]
Magnetic chitosan-polyvinyl alcohol blend (Fly ash modified)	0.564	123.8	30	4.0	0.6	200	[51]
Sawdust-based activated carbon	900	510.3	25	2.0	2.5	2000	[52]
SMS-700 °C	1011	120.4	22	6.0	1	1200	This work
SMS-900 °C	1095	168.1	22	6.0	1	1200	This work
SMS-700 °C + N	810	216.2	22	6.0	1	1200	This work
SMS-900 °C + N	943	392.9	22	6.0	1	1200	This work
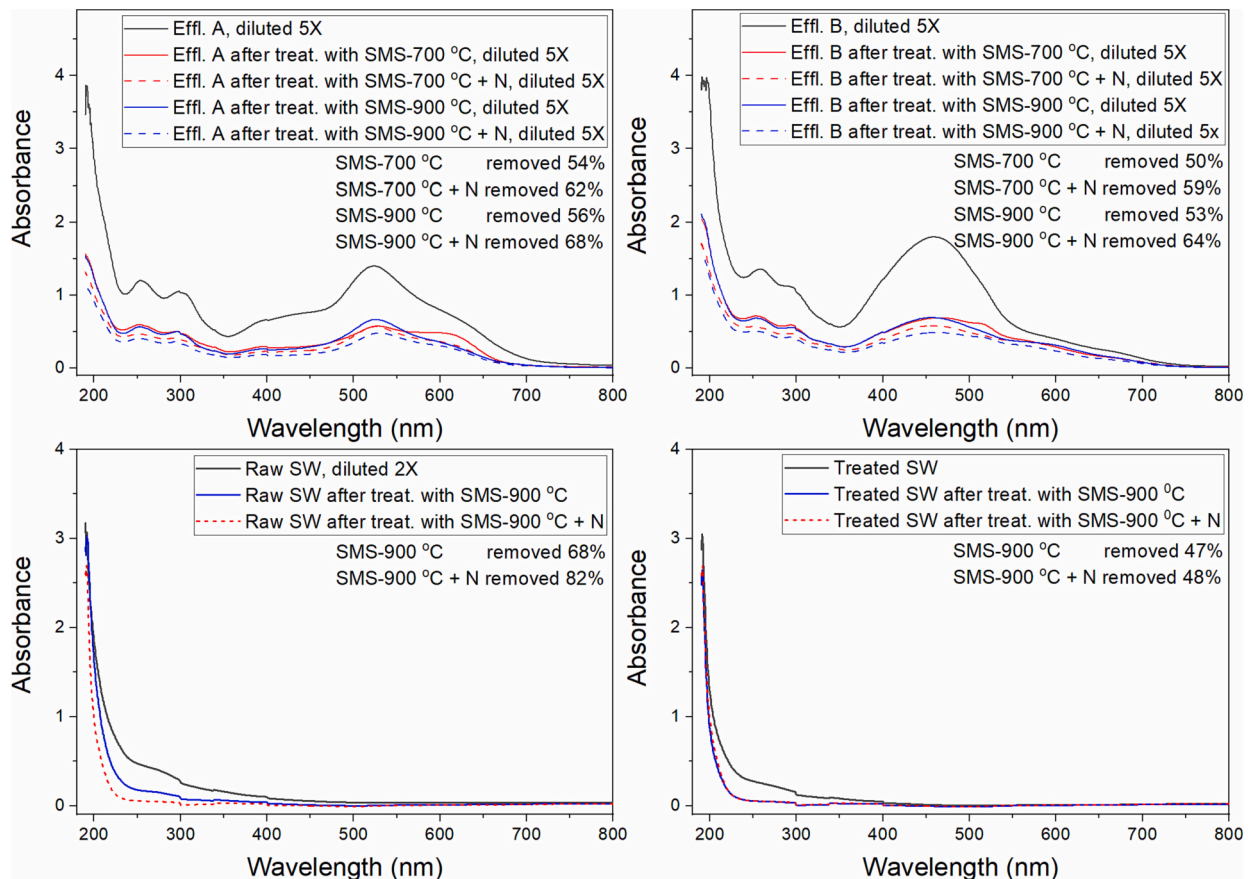
Fig. 9. Adsorption of contaminants from synthetic effluents and sewage water using SMS-based activated biochars. Conditions: temperature of 22 °C, initial pH of approximately 6.0 (effluent A and B), pH 7.2 (raw sewage water), pH 8.3 (treated sewage water), dosage of adsorbent 1 g/L.

doping/activation process was carried out in one step. Samples without the addition of melamine were used for comparison. Pyrolysis was carried out at 700 °C and 900 °C for 1 h. The produced biochars were tested for their performance during the removal of reactive orange-16 (RO-16) from water solutions, a mixture of contaminants from synthetic effluents, and real sewage water. Compared to the non-doped samples, the N-doped biochars had a lower SSA, more defective carbon structures, and a larger number of N-functionalities on their surface. For both the non-doped and N-doped biochars, the removal of RO-16

was strongly affected by the pH. The kinetics of adsorption were well represented by the Avrami fractional order model, and the adsorption isotherms were well fitted to the Liu model. The maximum adsorption capacities (q_{max}) of RO-16 were higher for the N-doped biochars, i.e., 120 mg/g (SMS-700 °C), 216 mg/g (SMS-700 °C + N), 168 mg/g (SMS-900 °C), and 393 mg/g (SMS-900 °C + N). The mechanism of adsorption of RO-16 is ruled by the pore filing process, electrostatic interactions, hydrogen bonding, and π-π and Lewis acid-base interactions. N-doped biochars were more effective for the removal of contaminants from

synthetic effluents and sewage water. N-doped biochar produced at 900 °C showed good recyclability.

Declaration of competing interest

The authors declare the following financial interests/personal relationships which may be considered as potential competing interests: Alejandro Grimm reports financial support was provided by Swedish Research Council Formas.

Data availability

Data will be made available on request.

Appendix A. Supplementary data

Supplementary data to this article can be found online at https://doi.org/10.1016/j.jwpe.2023.104435.

References

[1] International Council on Clean Transportation (ICCT), Availability of Cellulosic Residues and Wastes in the EU. https://theicct.org/publications/availability-cellulosic-residues-and-wastes-eu, 2016. (Accessed 1 August 2023).

[2] A. Grimm, G.S. dos Reis, V.M. Dinh, S.H. Larsson, J.-P. Mikkola, E.C. Lima, S. Xiong, Hardwood spent mushroom substrate–based activated biochar as a sustainable bioresource for removal of emerging pollutants from wastewater, Biomass Convers. Biorefin. (2022), https://doi.org/10.1007/s13399-022-02618-7.

[3] D. Royse, J.J.P. Baars, Q. Tan, Current overview of mushroom production in the world, in: D. Zied, A. Pardo-Giménez (Eds.), Edible and Medecianal Mushrooms: Technology and Applications, Wiley, Singapore, 2017, pp. 5–13.

[4] K.N. Finney, C. Ryu, V.N. Sharifi, J. Swithenbank, The reuse of spent mushroom compost and coal tailings for energy recovery: comparison of thermal treatment technologies, Bioresour. Technol. 100 (2009) 310–315, https://doi.org/10.1016/j.biortech.2008.05.054.

[5] F. Chen, S.J. Xiong, J. Sundelin, C. Martin, M. Hultberg, Potential for combined production of food and biofuel: cultivation of *Pleurotus pulmonarius* on soft- and hardwood sawdusts, J. Clean. Prod. 266 (2020), 122011, https://doi.org/10.1016/j.jclepro.2020.122011.

[6] A. Tkaczyk, K. Mitrowska, A. Posyniak, Synthetic organic dyes as contaminants of the aquatic environment and their implications for ecosystems: a review, Sci. Total Environ. 717 (2020), 137222, https://doi.org/10.1016/j.scitotenv.2020.137222.

[7] B. Lellis, C.Z. Fávaro-Polonio, J.A. Pamphile, J.C. Polonio, Effects of textile dyes on helth and the environment and bioremediation potential of living organisms, Biotechnol. Res. Innov. 3 (2019) 275–290, https://doi.org/10.1016/j.biori.2019.09.001.

[8] I. Bisschops, H. Spanjers, Literature review on textile wastewater characterisation, Environ. Technol. 24 (2003) 1399–1411, https://doi.org/10.1080/09593330309385684.

[9] S. Sandhya, Biodegradation of azo dyes under anaerobic condition: role of azoreductase, in: H.A. Erkurt (Ed.), Biodegradation of Azo Dyes. The Handbook of Environmental Chemistry vol. 9, Springer, Berlin, Heidelberg, 2010, pp. 39–57.

[10] M.M. Hassan, C.M. Carr, A critical review on recent advancements of the removal of reactive dyes from dyehouse effluent by ion-exchange adsorbents, Chemosphere 209 (2018) 201–219, https://doi.org/10.1016/j.chemosphere.2018.06.043.

[11] K. Rehman, T. Shahzad, A. Sahar, S. Hussain, F. Mahmood, M.H. Siddique, M. A. Siddique, M.I. Rashid, Effect of reactive black 5 azo dye on soil processes related to C and N cycling, PeerJ 6 (2018), e4802, https://doi.org/10.7717/peerj.4802.

[12] R.O. Alves de Lima, A.P. Bazo, D.M.F. Salvadori, C.M. Rech, D. de Palma Oliveira, G. de Aragão Umbuzeiro, Mutagenic and carcinogenic potential of a textile azo dye processing plant effluent that impacts a drinking water source, Mutat. Res. Genet. Toxicol. Environ. Mutagen. 626 (2007) 53–60, https://doi.org/10.1016/j.mrgentox.2006.08.002.

[13] K.T. Chung, Azo dyes and human health: a review, J. Environ. Sci. Health C 34 (2016) 233–261, https://doi.org/10.1080/10590501.2016.1236602.

[14] K. Golka, S. Kopps, Z.W. Myslak, Carcinogenicity of azo colorants: influence of solubility and bioavailability, Toxicol. Lett. 151 (2004) 203–210, https://doi.org/10.1016/j.toxlet.2003.11.016.

[15] M.S. Islam, B.C. Ang, S. Gharehkhani, A.B.M. Afifi, Adsorption capability of activated carbon synthesized from coconut shell, Carbon Lett. 20 (2016) 1–9, https://doi.org/10.5714/CL.2016.20.001.

[16] V.K. Suhas, L.P. Gupta, M. Singh, S. Kushwaha Chaudhary, A novel approach to develop activated carbon by an ingenious hydrothermal treatment methodology using Phyllanthus emblica fruit stone, J. Clean. Prod. 288 (2021), 125643, https://doi.org/10.1016/j.jclepro.2020.125643.

[17] F. Márquez-Montesino, N. Torres-Figueredo, A. Lemus-Santana, F. Trejo, Activated carbon by potassium carbonate activation from pine sawdust (Pinus montezumae Lamb.), Chem. Eng. Technol. 43 (2020) 1716–1725, https://doi.org/10.1002/ceat.202000051.

[18] Z. Liu, F. Zhang, T. Liu, N. Peng, C. Gai, Removal of azo dye by a highly graphitized and heteroatom doped carbon derived from fish waste: adsorption equilibrium and kinetics, J. Environ. Manag. 182 (2016) 446–454, https://doi.org/10.1016/j.jenvman.2016.08.008.

[19] X. Peng, X. Hu, D. Fu, F.L.Y. Lam, Adsorption removal of acid black 1 from aqueous solution using ordered mesoporous carbon, Appl. Surf. Sci. 294 (2014) 71–80, https://doi.org/10.1016/j.apsusc.2013.11.157.

[20] F. Chen, C. Martín, T.A. Lestander, A. Grimm, S. Xiong, Shiitake cultivation as biological preprocessing of lignocellulosic feedstocks – substrate changes in crystallinity, syringyl/guaiacyl lignin and degradation-derived by-products, Bioresour. Technol. 344 (2022), 126256, https://doi.org/10.1016/j.biortech.2021.126256.

[21] M. Thommes, K. Kaneko, A.V. Neimark, J.P. Olivier, F. Rodriguez-Reinoso, J. Rouquerol, Physisorption of gases, with special reference to the evaluation of surface area and pore size distribution (IUPAC technical report), Pure Appl. Chem. 87 (2015) 1051–1069.

[22] G.S. dos Reis, S.H. Larsson, M. Thyrel, M. Mathieu, P.N. Tung, Application of design of experiments (DoE) for optimised production of micro-and mesoporous Norway spruce bark activated carbons, Biomass Convers. Biorefin. (2021), https://doi.org/10.1007/s13399-021-01917-9.

[23] G.S. dos Reis, E.C. Lima, C.H. Sampaio, F.S. Rodembusch, C.O. Petter, B. G. Cazacliu, G.L. Dotto, G.E.N. Hidalgo, Novel kaolin/ polysiloxane based organicinorganic hybrid materials: sol-gel synthesis, characterisation, and photocatalytic properties, J. Solid State Chem. 260 (2018) 106–116.

[24] G.S. dos Reis, D. Bergna, A. Grimm, E.C. Lima, H. Hu, M. Naushad, U. Lassi, Preparation of highly porous nitrogen-doped biochar derived from birch tree wastes with superior dye removal performance, Colloids Surf. A 669 (2023), 131493, https://doi.org/10.1016/j.colsurfa.2023.131493.

[25] M. González-Hourcade, G. Simões dos Reis, A. Grimm, V.M. Dinh, E.C. Lima, S. H. Larsson, F.G. Gentili, Microalgae biomass as a sustainable precursor to produce nitrogen-doped biochar for efficient removal of emerging pollutants from aqueous media, J. Clean. Prod. 348 (2022), 131280, https://doi.org/10.1016/j.jclepro.2022.131280.

[26] J.R. Pels, F. Kapteijn, J.A. Moulijn, Q. Zhu, K.M. Thomas, Evolution of nitrogen functionalities in carbonaceous materials during pyrolysis, Carbon 33 (1995) 1641–1653, https://doi.org/10.1016/0008-6223(95)00154-6.

[27] A.P. Terzyk, The influence of activated carbon surface chemical composition on the adsorption of acetaminophen (paracetamol) in vitro, part II. TG, FTIR, and XPS analysis of carbons and the temperature dependence of adsorption kinetics at the neutral pH, Colloids Surf. A 177 (2001) 23–45, https://doi.org/10.1016/S0927-7757(00)00594-X.

[28] A.A. Oladipo, A.O. Ifebajo, Highly efficient magnetic chicken bone biochar for removal of tetracycline and fluorescent dye from wastewater: two-stage adsorber analysis, J. Environ. Manag. 209 (2018) 9–16, https://doi.org/10.1016/j.jenvman.2017.12.030.

[29] A.A. Oladipo, A.O. Ifebajo, N. Nisar, O.A. Ajayi, High-performance magnetic chicken bone-based biochar for efficient removal of rhodamine-B dye and tetracycline: competitive sorption analysis, Water Sci. Technol. 76 (2017) 373–385, https://doi.org/10.2166/wst.2017.209.

[30] A. Roy, S. Chakraborty, S.P. Kundu, B. Adhikari, S.B. Majumder, Adsorption of anionic-azo dye from aqueous solution by lignocellulose-biomass jute fiber: equilibrium, kinetics, and thermodynamics study, Ind. Eng. Chem. Res. 51 (2012) 12095–12106, https://doi.org/10.1021/ie301708e.

[31] G.S. dos Reis, J. Thivet, E. Laisné, V. Srivastava, A. Grimm, E.C. Lima, D. Bergna, T. Hu, M. Naushad, U. Lassi, Synthesis of novel mesoporous selenium-doped biochar with high-performance sodium diclofenac and reactive orange 16 dye removals, Chem. Eng. Sci. 119129 (2023), https://doi.org/10.1016/j.ces.2023.119129.

[32] P.S. Thue, R.A. Teixeira, E.C. Lima, B.L. Mello, G.S. dos Reis, F.M. Machado, S. Hussain, H. Khan, N. Hussain, M. Naushad, Surface modification of natural clay with H2O2 for high adsorption of acid red 114: experimental and modelling studies, J. Mol. Liq. 388 (2023), 122740, https://doi.org/10.1016/j.molliq.2023.122740.

[33] R. Muralikrishnan, C. Jodhi, Biodecolorization of Reactive Orange 16 using biochar produced from groundnut shell (*Arachis hypogaea*): batch, isotherm, kinetic, and regeneration studies, Biomass Convers. Biorefin. (2021), https://doi.org/10.1007/s13399-021-01710-8.

[34] R. Ahmad, R. Kumar, Adsorptive removal of Congo red dye from aqueous solution using bael shell carbon, Appl. Surf. Sci. 257 (2010) 1628–1633, https://doi.org/10.1016/j.apsusc.2010.08.111.

[35] E.C. Lima, M.A. Adebayo, F.M. Machado, C.P. Bergmann, F.M. Machado (Eds.), Springer (2015) 33–69.

[36] E.C. Lima, M.H. Dehghani, A. Guleria, F. Sher, R.R. Karri, G.L. Dotto, H.N. Tran, Adsorption: fundamental aspects and applications of adsorption for effluent treatment, in: M. Hadi Dehghani, R. Karri, É. Lima (Eds.), Green Technologies for the Defluoridation of Water, Elsevier, Amsterdam, 2021, pp. 41–88.

[37] N.F.G.M. Cimirro, E.C. Lima, M.R. Cunha, P.S. Thue, A. Grimm, G.S. dos Reis, N. Rabiee, M.R. Saeb, F. Keivanimehr, S. Habibzadeh, Removal of diphenols using pine biochar, kinetics, equilibrium, thermodynamics and mechanism of uptake, J. Mol. Liq. 364 (2022), 119979, https://doi.org/10.1016/j.molliq.2022.119979.

[38] G.L. Dotto, J. Vieillard, D. Pinto, S.F. Lütke, L.F.O. Silva, G.S. dos Reis, E.C. Lima, D.S.P. Franco, Selective adsorption of gadolinium from real leachate using a natural bentonite clay, J. Environ. Chem. Eng. 11 (2023), 109748, https://doi.org/10.1016/j.jece.2023.109748.

[39] M.C. Ribas, M.A.E. de Franco, M.A. Adebayo, E.C. Lima, G.M.B. Parkes, L.A. Feris, Adsorption of Procion Red MX-5B dye from aqueous solution using homemade peach and commercial activated carbons, Appl Water Sci 10 (2020) 154, https://doi.org/10.1007/s13201-020-01237-9.

[40] E.H.M. Cavalcante, L.C.M. Candido, H.P. de Oliveira, K. Barreto Silveira, T.V. de Souza Álvares, E.C. Lima, M. Thyrel, S.H. Larsson, G.S. dos Reis, 3-Aminopropyl-triethoxysilane-functionalized tannin-rich grape biomass for the adsorption of methyl orange dye: synthesis, characterization, and the adsorption mechanism, ACS Omega 7 (2022) 18997–19009, https://doi.org/10.1021/acsomega.2c02101.

[41] T. Calvete, E.C. Lima, N.F. Cardoso, J.C.P. Vaghetti, S.L.P. Dias, F.A. Pavan, Application of carbon adsorbents prepared from Brazilian-pine fruit shell for the removal of reactive orange 16 from aqueous solution: kinetic, equilibrium, and thermodynamic studies, J. Environ. Manag. 91 (2010) 1695–1706, https://doi.org/10.1016/j.jenvman.2010.03.0.

[42] G.S. dos Reis, M. Guy, M. Mathieu, M. Jebrane, E.C. Lima, M. Thyrel, G.L. Dotto, S.H. Larsson, A comparative study of chemical treatment by MgCl2, ZnSO4, ZnCl2, and KOH on physicochemical properties and acetaminophen adsorption performance of biobased porous materials from tree bark residues, Colloids Surf. A Physicochem. Eng. Asp. 642 (2022), 128626, https://doi.org/10.1016/j.colsurfa.2022.128626.

[43] G.S. dos Reis, D. Pinto, E.C. Lima, S. Knani, A. Grimm, L.F.O. Silva, T.R.S. Cadaval Jr., G.L. Dotto, Lanthanum uptake from water using chitosan with different configurations, React. Funct. Polym. 180 (2022), 105395, https://doi.org/10.1016/j.reactfunctpolym.2022.105395.

[44] A.S. Abdulhameed, A.T. Mohammad, A.H. Jawad, Application of response surface methodology for enhanced synthesis of chitosan tripolyphosphate/TiO2 nanocomposite and adsorption of reactive orange 16 dye, J. Clean. Prod. 232 (2019) 43–56, https://doi.org/10.1016/j.jclepro.2019.05.291.

[45] F. Marrakchi, M.J. Ahmed, W.A. Khanday, M. Asif, B.H. Hameed, Mesoporous carbonaceous material from fish scales as low-cost adsorbent for reactive orange 16 adsorption, J. Taiwan Inst. Chem. E. 71 (2017) 47–54, https://doi.org/10.1016/j.jtice.2016.12.026.

[46] D. Castro dos Santos, M. Ayorinde Adebayo, S. de Fátima Pinheiro Pereira, L.D. Tentler Prola, R. Cataluña, E.C. Lima, C. Saucier, C. Rodrigues Gally, F. Machado Machado, New carbon composite adsorbents for the removal of textile dyes from aqueous solutions: kinetic, equilibrium, and thermodynamic studies, Korean J. Chem. Eng. 31 (2014) 1470–1479, https://doi.org/10.1007/s11814-014-0086-3.

[47] M. Auta, B.H. Hameed, Optimized and functionalized paper sludge activated with potassium fluoride for single and binary adsorption of reactive dyes, J. Ind. Eng. Chem. 20 (2014) 830–840, https://doi.org/10.1016/j.jiec.2013.06.013.

[48] G. Kavitha, P. Subhapriya, V. Dhanapal, G. Dineshkumar, V. Venkateswaran, Dye removal kinetics and adsorption studies of activated carbon derived from the stems of Phyllanthus reticulatus, Mater. Today Proc. 45 (2021) 7934–7938, https://doi.org/10.1016/j.matpr.2020.12.837.

[49] N.N.A. Malek, A.H. Jawad, A.S. Abdulhameed, K. Ismail, B.H. Hameed, New magnetic Schiff's base-chitosan-glyoxal/fly ash/Fe3O4 biocomposite for the removal of anionic azo dye: an optimized process, Int. J. Biol. Macromol. 146 (2020) 530–539, https://doi.org/10.1016/j.ijbiomac.2020.01.020.

[50] S.W. Won, S.B. Choi, Y.S. Yun, Performance and mechanism in binding of Reactive Orange 16 to various types of sludge, Biochem. Eng. J. 28 (2006) 208–214, https://doi.org/10.1016/j.bej.2005.11.006.

[51] N.N.A. Malek, A.H. Jawad, K. Ismail, R. Razuan, Z.A. ALOthman, Fly ash modified magnetic chitosan-polyvinyl alcohol blend for reactive orange 16 dye removal: adsorption parametric optimization, Int. J. Biol. Macromol. 189 (2021) 464–476, https://doi.org/10.1016/j.ijbiomac.2021.08.160.

[52] K. Vijayaraghavan, S.W. Won, Y.-S. Yun, Treatment of complex Remazol dye effluent using sawdust- and coal-based activated carbons, J. Hazard. Mater. 167 (2009) 790–796, https://doi.org/10.1016/j.jhazmat.2009.01.055.

[53] F.G. Gentili, J. Fick, Algal cultivation in urban wastewater: an efficient way to reduce pharmaceutical pollutants, J. Appl. Phycol. 29 (2017) 255–262, https://doi.org/10.1007/s10811-016-0950-0.

[54] R.H. Lindberg, S. Namazkar, S. Lage, M. Östman, Z. Gojkovic, C. Funk, F.G. Gentili, M. Tysklind, Fate of active pharmaceutical ingredients in a northern high-rate algal pond fed with municipal wastewater, Chemosphere 271 (2021), 129763, https://doi.org/10.1016/j.chemosphere.2021.129763.